Journal of Structural Geology 125 (2019) 319–324

Contents lists available at ScienceDirect

Journal of Structural Geology

journal homepage: www.elsevier.com/locate/jsg

Slate – A new record for crystal preferred orientation

Hans-Rudolf Wenk[a,*], Waruntorn Kanitpanyacharoen[b], Yang Ren[c]

[a] Department of Earth and Planetary Science, University of California, Berkeley, CA 94720, USA
[b] Department of Geology, Faculty of Science, Chulalongkorn University, Bangkok, Thailand
[c] X-ray Science Division, Advanced Photon Source, Argonne National Laboratory, Lemont, IL 60439, USA

ARTICLE INFO

Keywords:
Slate
Preferred orientation
Muscovite
Chlorite
Quartz

ABSTRACT

This report describes microstructures and preferred orientation of a Devonian slate from the Belgian Ardennes (La Fortelle quarry). The sample, composed largely of muscovite, chlorite, and quartz, displays extraordinary texture strength of muscovite, exceeding 100 multiples of random distribution (m.r.d.) for (001) pole figures and thus setting a new record for preferred orientation in rocks. Quantitative texture analysis was performed with the Rietveld method on synchrotron X-ray diffraction images. Interestingly, quartz also displays strong shape preferred orientation (SPO) as revealed by X-ray microtomography and SEM imaging but largely random crystallographic preferred orientation (CPO). Microstructural evidence suggests that this fine-grained rock formed by recrystallization of shale under stress, with growth of phyllosilicates and dissolution and growth of quartz.

1. Introduction

Twenty years ago van der Pluijm et al. (1998) wrote a challenging discussion "Contradictions of slate formation resolved?". We decided to return to this topic, highlighting some of the extraordinary properties of slate, particularly preferred orientation of component minerals in this fine-grained rock. Alignment of minerals in polycrystalline aggregates or "texture" was first introduced by Omalius d'Halloy (1833) in his book on structural geology. Since then "texture" has become universally adapted in materials science while structural geology prefers to refer to "crystal preferred orientation (CPO)" (e.g. Passchier and Trouw, 2005; page 2, Box 1.1). Here the two terms are used synonymously. The orientation of crystals relative to the sample is quantitatively described by the statistical orientation distribution function (ODF) that relates crystal coordinates to sample coordinates by three rotations. Texture and associated anisotropy of physical properties have become important topics in materials science, structural geology, and geophysics.

The strength of texture is described by comparing the ODF of a textured sample with the alignment in an aggregate with random preferred orientation (multiples of random distribution or m.r.d.). Sander (1950) provided a comprehensive compilation of mineral textures in deformed rocks, and quartz *c*-axis alignment in a recrystallized granulite from Saxony displayed a maximum with ~20 m.r.d. This was exceeded when Bunge (1969) introduced quantitative texture analysis and described a recrystallized aluminum wire with ~28 m.r.d. The texture type, described as cube texture resembling a single crystal, was referred to by Hutchinson (2012) as "a great wonder of nature" and can produce extreme alignment of > 1000 m.r.d. (Hutchinson and Nes, 1992). In geology Haerinck et al. (2015) observed a pole density maximum for muscovite (001) in slate from Brittany higher than 39 m.r.d. This provided the stimulus to further investigate these extraordinary rocks and here we describe textures and microstructures of a Devonian slate from the Belgian Ardennes with a (001) maximum of muscovite of 123 m.r.d. It is part of a more systematic survey of preferred orientation patterns in slates from a variety of geological settings.

Slates are distinguished from other rocks by their extraordinary cleavage and, because of this anisotropic property, have long been used for tiles in roofs and floors. There are detailed reviews of world-wide slate localities and the composition of these special rocks (e.g. Wagner et al., 1995; Cardenes et al., 2014) but there is not much information about the unique slate fabric. An extensive literature in structural geology discusses slaty cleavage (e.g. Ishii, 1988; Merriman et al., 1990; Tullis, 1976; Wood and Oertel, 1980). Slates are primarily composed of phyllosilicates (white mica, chlorite, and occasionally chloritoid) and quartz. They represent low-grade metamorphic recrystallized sedimentary shales. There are some studies of quantitative texture analysis using an X-ray pole figure goniometer, all emphasizing (001) pole figures of muscovite (e.g. Oertel, 1983; Oertel and Phakey, 1972; Ho et al., 2001). This method is limited by providing only incomplete pole figure coverage and difficulties in separating overlapping diffraction peaks, particularly for polyphase systems.

Applying new quantitative methods of texture analysis developed for shales (e.g. Wenk et al., 2014) to slates revealed extreme preferred

* Corresponding author.
E-mail address: wenk@berkeley.edu (H.-R. Wenk).

https://doi.org/10.1016/j.jsg.2017.12.009
Received 15 August 2017; Received in revised form 12 December 2017; Accepted 14 December 2017
Available online 16 December 2017
0191-8141/ © 2017 Elsevier Ltd. All rights reserved.

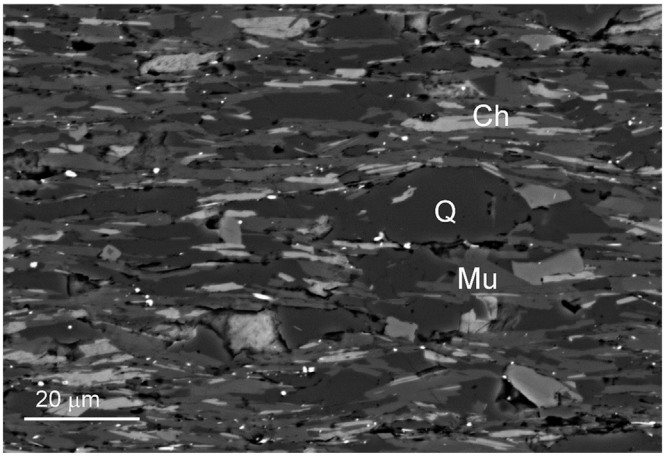

Fig. 1. Backscatter electron SEM image of La Fortelle slate. Polished section cut perpendicular to the foliation; foliation plane is horizontal. Dark is quartz (Q), medium gray is muscovite (Mu), light gray is chlorite (Ch), and white is pyrite and rutile.

orientation of muscovite, much stronger than that observed in shales and gneiss (e.g. Wenk et al., 2010). This report focuses on microstructures and orientation patterns of a slate from the La Fortelle quarry in the Belgian Ardennes (e.g. Voisin, 1987; Schavemaker et al., 2012), investigating the fabric with scanning electron microscopy (SEM), shape preferred orientation (SPO) with synchrotron X-ray microtomography, and crystallographic preferred orientation (CPO) patterns with high energy synchrotron X-ray diffraction.

2. Experimental methods and results

A sample slab was polished and carbon-coated for scanning electron microscope (SEM) investigations and examined with a Zeiss Evo MA10 SEM equipped with an EDAX energy-dispersive spectroscopy (EDS) system at the University of California, Berkeley. The brightness variations of the backscattered (BE) SEM image (Fig. 1), ranging from low (black) to high (white), is mainly due to the contrast in atomic number. Bright gray grains correspond to chlorite with high atomic numbers, intermediate shades are muscovite, and darker areas represent quartz. The brightest white spots are pyrite and rutile. EDS was employed to identify phases based on chemical composition. There are minor components of calcite and apatite. In the section perpendicular to the foliation, the grain size ranges from ~10 to 20 μm in length to ~1–5 μm in thickness with 2D aspect ratios for most grains, including phyllosilicates and quartz, at ~5:1.

In order to explore the three-dimensional microstructures of component minerals, particularly shape preferred orientation (SPO), phase proportion, and aspect ratio, a cylindrical piece was analyzed by synchrotron X-ray microtomography at beamline 8.3.2 of the Advanced Light Source (ALS) of Lawrence Berkeley National Laboratory. A monochromatic X-ray with an energy of 18 keV was used to penetrate through a 1 mm diameter cylindrical sample and record digital radiographs on a CCD detector (2048 × 2048 pixels). The sample was continuously rotated in 0.12° increments until radiographs representing ~180° of rotation were collected. A total of 1500 tomographic radiographs were obtained and each radiograph exposure was 2 s, thus a full 3D tomographic data collection takes ~30 min. A 10× optical lens was used in the measurements to obtain a high spatial resolution of ~0.65 μm/pixel. A volume of interest of 260 × 260 × 80 μm^3 was selected for data segmentation of SPO, phase proportion, and 3D aspect ratio. More details of data collection and analysis are described in

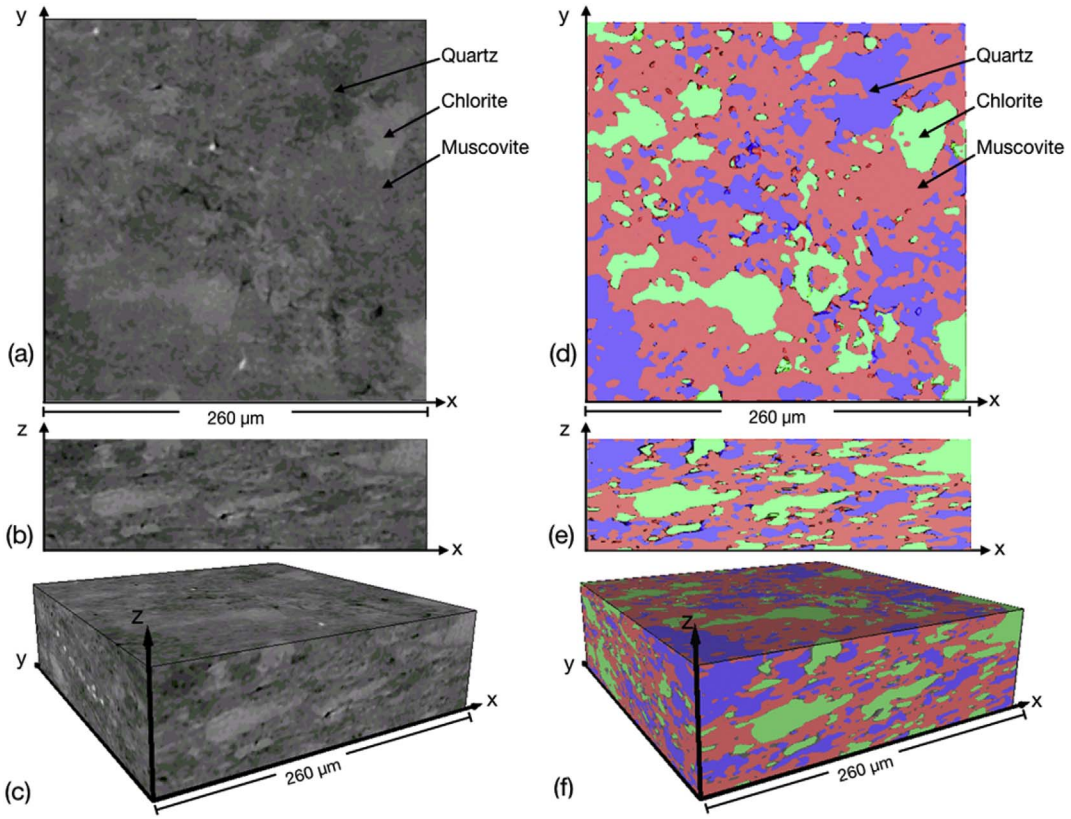

Fig. 2. X-ray microtomography of slate. (a–c): gray shades illustrating different X-ray absorption values of phases. (d–f): segmentation into minerals includes quartz (purple), chlorite (green), and muscovite (orange). Pore and pyrite are present in low amounts (white dots in a–c). The cleavage plane is roughly in the xy plane. (For interpretation of the references to color in this figure legend, the reader is referred to the Web version of this article.)

Kanitpanyacharoen et al. (2013).

The software Avizo (FEI Visualization Sciences Group) was used for segmentation and graphical representation. Grayscales or X-ray absorption values of tomographic images range from −18 to 100 and can be distinctively segmented into five phases: pore, quartz, muscovite, chlorite, and pyrite, in the order from low to high grayscale values, respectively. High X-ray absorbing materials such as pyrite and chlorite, which contain a significant amount of iron, appear bright in the images whereas low absorbing materials such as quartz and muscovite appear in dark gray tones (Fig. 2a–c). Pore and pyrite are present in low amounts (< 1 vol%) and are not the focus of this study. Fig. 2d–f display the 2D and 3D microstructures of muscovite (orange), chlorite (green), and quartz (purple) which are the main phases of this slate. Quartz is the most abundant phase and constitutes 49 vol% while muscovite composes 28 vol% and chlorite 23 vol%. The 2D reconstructed image (Fig. 2a) and segmented data (Fig. 2d) display complex and irregular shapes of constituent minerals in the xy plane that corresponds roughly to the cleavage plane. Conversely, in the xz (Fig. 2b, e) and yz planes (not shown), the shapes of quartz, chlorite, and muscovite are elongated and more or less parallel to the cleavage plane. The 3D reconstruction and segmentation of the sample clearly shows strong shape preferred orientation of all three minerals (Fig. 2c, f). The average 3D aspect ratios of muscovite, chlorite, and quartz are 2.7, 2.9, and 2.7, respectively. Note that the calculation of aspect ratio excludes grains that are smaller than 20 μm^3. These aspect ratios are smaller than estimates from the SEM image which may be related to the limited resolution of tomography or the fact that a different region of the sample was explored.

Another small cylinder, approximately 2 mm in diameter and 10 mm long, with the axis perpendicular to the cleavage plane, was prepared for synchrotron high-energy X-ray diffraction experiments conducted at beamline 11-ID-C of the Advanced Photon Source (APS) of Argonne National Laboratory. A monochromatic X-ray beam with a wavelength of 0.10789 Å (114.9 KeV), was collimated to 1 × 1 mm and the sample was analyzed in transmission mode. During X-ray exposure, the sample was translated over 2 mm along the horizontal axis (and perpendicular to the cleavage plane) to cover a representative sample volume and adequate grain statistics. Diffraction images were recorded with a Perkin Elmer amorphous silicon detector (2048 × 2048 pixels) positioned about 2 m away from the sample. Fig. 3a displays a diffraction image and Fig. 4 shows a corresponding diffraction pattern obtained by an azimuthal average of a diffraction image, illustrating the multiphase composition. In the diffraction image (Fig. 3a), X-ray intensity variations along Debye-rings are indicative of texture; for example the (002) peak of muscovite and (001) peak of chlorite show a strong maximum in the horizontal direction that is perpendicular to the foliation/cleavage plane. In contrast, diffraction rings for quartz display almost uniform intensity (e.g. (100) peak)). Note that the apparent intensity differences in the quartz (101) peak (at 2θ = 1.9°) are due to superposition with the muscovite (006) peak (Fig. 3b). Seven images were recorded by rotating the sample around the horizontal axis, from −90° to 90° in 30° increments, to provide adequate orientation coverage for texture analysis. Each image was integrated over 10° azimuthal sectors to obtain a total of 36 diffraction patterns.

The X-ray diffraction patterns (in total 36 × 7 = 252), with a 2θ range from 0.4° to 5.0° (d range 24 Å-1.3 Å) were then analyzed by the Rietveld method (Rietveld, 1969) implemented in the software MAUD and described in detail by Lutterotti et al. (2014) and Wenk et al. (2014). A polynomial function with five coefficients was used to refine the background of each image and three minerals were considered, with corresponding crystallographic information from the literature: 2M-muscovite (Guggenheim et al., 1987; amcsd 0001076), quartz (Antao et al., 2008; amcsd 0006212), and monoclinic chlorite (Zanazzi et al., 2007; amcsd 0004284). Refined parameters include instrument geometry, lattice parameters of phases, grain size, volume fractions of phases, and the crystallographic preferred orientation distribution (OD). Fig. 3b shows a stack of measured diffraction spectra (bottom) and corresponding Rietveld fits (top). There is excellent agreement between the measured and modeled spectra, giving confidence in the refinement. The Rietveld refinement determines phase proportions to be 36 vol% muscovite, 17 vol% chlorite, and 47 vol% quartz, similar to the microtomography results.

The ODs were obtained from variations in diffraction intensities with the method WIMV (Matthies and Vinel, 1982), using a 5° grid for muscovite and chlorite and a 10° grid for quartz. The ODs were exported from MAUD and introduced into BEARTEX (Wenk et al., 1998) to rotate the sample such that the center of the pole figure is the normal to the cleavage plane, and to calculate and plot pole figures (Fig. 5). There is very strong alignment of (001) planes of muscovite and chlorite in the foliation plane, but b = (010) poles rotate freely in the (001) plane. Quite surprising is the absence of significant crystallographic preferred orientation of quartz, in spite of strong shape preferred orientation. Table 1 summarizes OD maxima and (001) pole figure maxima and minima for the main phases.

3. Discussion

In the introduction it was mentioned that the (001) muscovite texture of fine-grained La Fortelle slate with three major components exceeds any other recorded polycrystal texture in rocks with a maximum of 123 m.r.d.. The alignment of (001) muscovite and chlorite platelets in the cleavage plane is very high (Table 1). For muscovite the

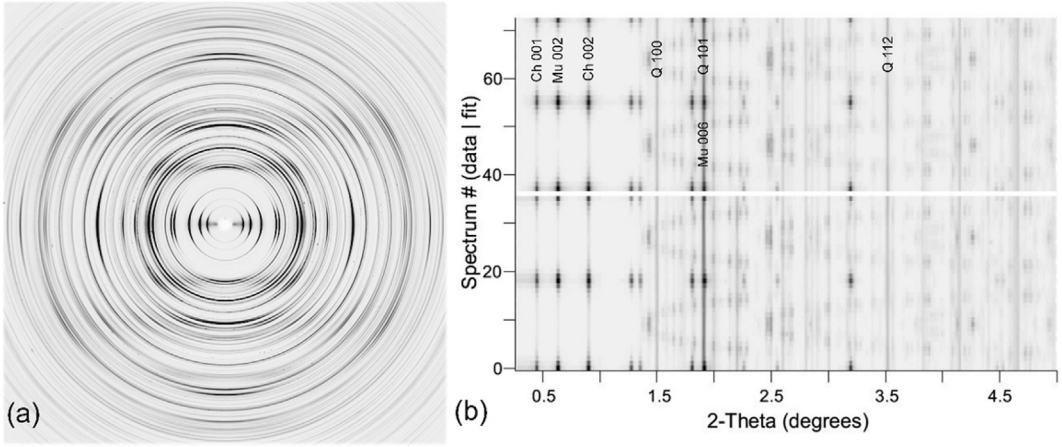

Fig. 3. (a) X-ray diffraction image. Foliation plane is vertical. (b) Stack of 36 diffraction spectra integrated over 10° sectors, corresponding to (a), bottom: experimental spectra, top: Rietveld refinement. Some diffraction peaks are indexed: Q is quartz, Mu is muscovite, and Ch is chlorite.

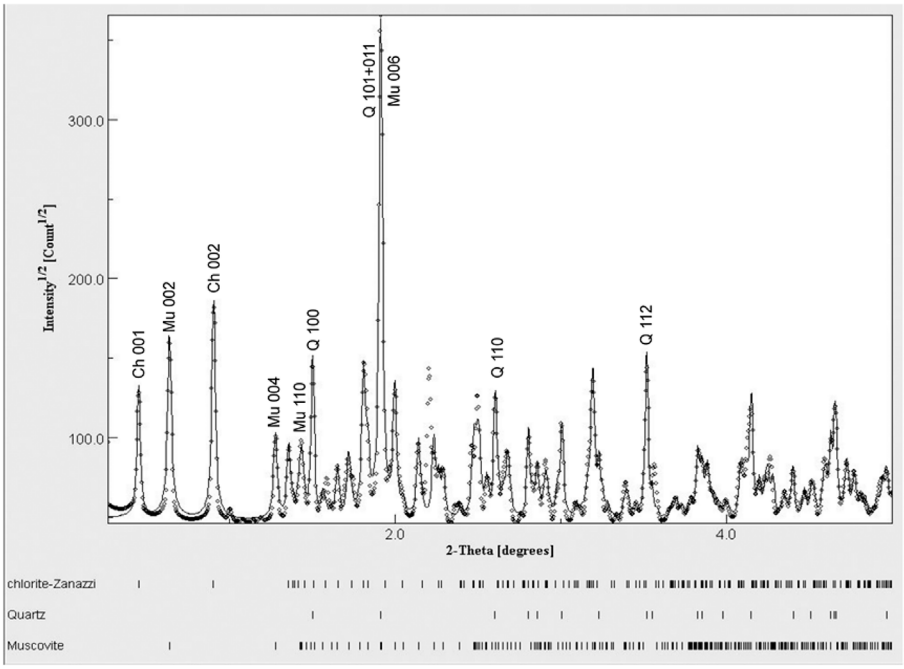

Fig. 4. X-ray diffraction pattern of slate with some peak identifications: Q is quartz, Mu is muscovite, and Ch is chlorite. This pattern is an azimuthal average over the diffraction images in Fig. 3a. Note that the dots outline the experimental profile and the black line is the refinement.

measured width of the (001) pole figure maximum at half the full intensity is 5.2°, which should be considered a maximum, partially due to the ODF resolution (5°), azimuthal averaging (10°) and limited pole figure coverage. The *b*-axes (or (010) poles) rotate freely in the cleavage plane, consistent with microtomography data that show no evidence of a morphologic lineation.

How does such an extraordinary pattern develop? One interpretation of slate texture (e.g. Oertel, 1983) has been mechanical rotation of rigid platy particles deforming in a viscous matrix, like a stack of cards (Jeffery, 1923; March, 1932) and this concept has been applied to derive plastic strain during deformation of an aggregate. It may be applicable to phyllosilicates in shales but is unlikely for slates where microstructures indicate growth during recrystallization (Fig. 1). The crystal orientation during growth under stress is controlled by thermodynamic considerations, especially for single crystals with highly anisotropic elastic properties (e.g. Kamb, 1959; Paterson, 1973; Shimizu, 1992). This provides a mechanism for the strong alignment of muscovite and chlorite particles. The stiffness of muscovite ranges from 58 to 187 GPa (Vaughan and Guggenheim, 1986) and for chlorite from 54 to 186 GPa (Aleksandrov and Ryzhova, 1961), with the softest direction perpendicular to (001). It should be mentioned that also the crystallinity of muscovite and chlorite is very high, with sharp X-ray peaks and width at half maximum of 0.022° 2θ for (002) muscovite and 0.025° for (001) chlorite, comparable to (100) quartz (0.022°) and indicative of equilibrium crystallization (e.g. Eberl and Velde, 1989; Merriman et al., 1990; Warr and Cox, 2016).

The random CPO of quartz is more difficult to explain. Quartz and phyllosilicates are the main components of shales from which slates formed and during this transformation there has been large grain growth. Quartz grows to similar and even larger size than muscovite. Perhaps the lack of significant CPO is due to the much lower single crystal elastic anisotropy with stiffness of quartz crystals ranging from 76 to 128 GPa (Ohno et al., 2006). The shape preferred orientation (SPO) of quartz may be caused by pressure solution (e.g. Plessmann, 1966; Powell, 1972; Durney, 1976; Rutter, 1976; Engelder et al., 1980), though in the case of this sample no dependence of crystal shape with crystal orientation could be established. Quartz may dissolve as a result of pressure solution and reprecipitate in between phyllosilicate grains. . The Devonian slate may have undergone more than one recrystallization event (e.g. Schavemaker et al., 2012) and locally was subjected to secondary deformation inducing kinking, but not in this sample.

This example described here may inspire others to apply the new quantitative methods for determining CPO and SPO to a wide range of slate problems, as already stipulated by van der Pluijm et al. (1998), for example, to document changes during the transition from shales to slates (e.g. Powell, 1972; Ishii, 1988; Merriman et al., 1990), effects of subsequent deformations imposed on the original slate fabric (e.g. Wood and Oertel, 1980; Knipe, 1981; Van Noten et al., 2012), and the transformation of slates to schists during high temperature metamorphism (e.g. Siddans, 1979; Ortoleva et al., 1982). Not all slates show extreme texture strength as the La Fortelle sample. Of about a dozen randomly selected slates in a preliminary survey all show strong CPO, some coming close to the sample described here, while others range from 20 to 40 m.r.d. The reasons for this need to be explored in the future.

4. Conclusions

The slate investigated in this study shows striking evidence of extreme preferred orientation of phyllosilicates that could only be quantified with new synchrotron X-ray diffraction methods and corresponding Rietveld data analysis. Equally surprising has been the virtual absence of crystallographic preferred orientation in highly flattened quartz. In the future a wide range of slates from the Belgian Ardennes and also from different geologic environments should be explored, to better understand the details of the microstructural evolution, including the transition from shale to slate during diagenesis and low-grade metamorphism. Experimental methods and data analysis are straightforward and can be applied to this fascinating system.

Acknowledgements

HRW acknowledges support from NSF (EAR-1343908) and DOE (DE-FG02-05ER15637). WK acknowledges support from Thailand Research Fund (TRG5880240) and the Development New Faculty Staff, Rachaphiseksomphot Endowment Fund. The diffraction experiment was conducted at beamline 11-ID-C of the Advanced Photon Source, a U.S. Department of Energy Office of Science User Facility operated for the DOE Office of Science by Argonne National Laboratory under Contract No. DE-AC02-06CH11357. The microtomography experiment

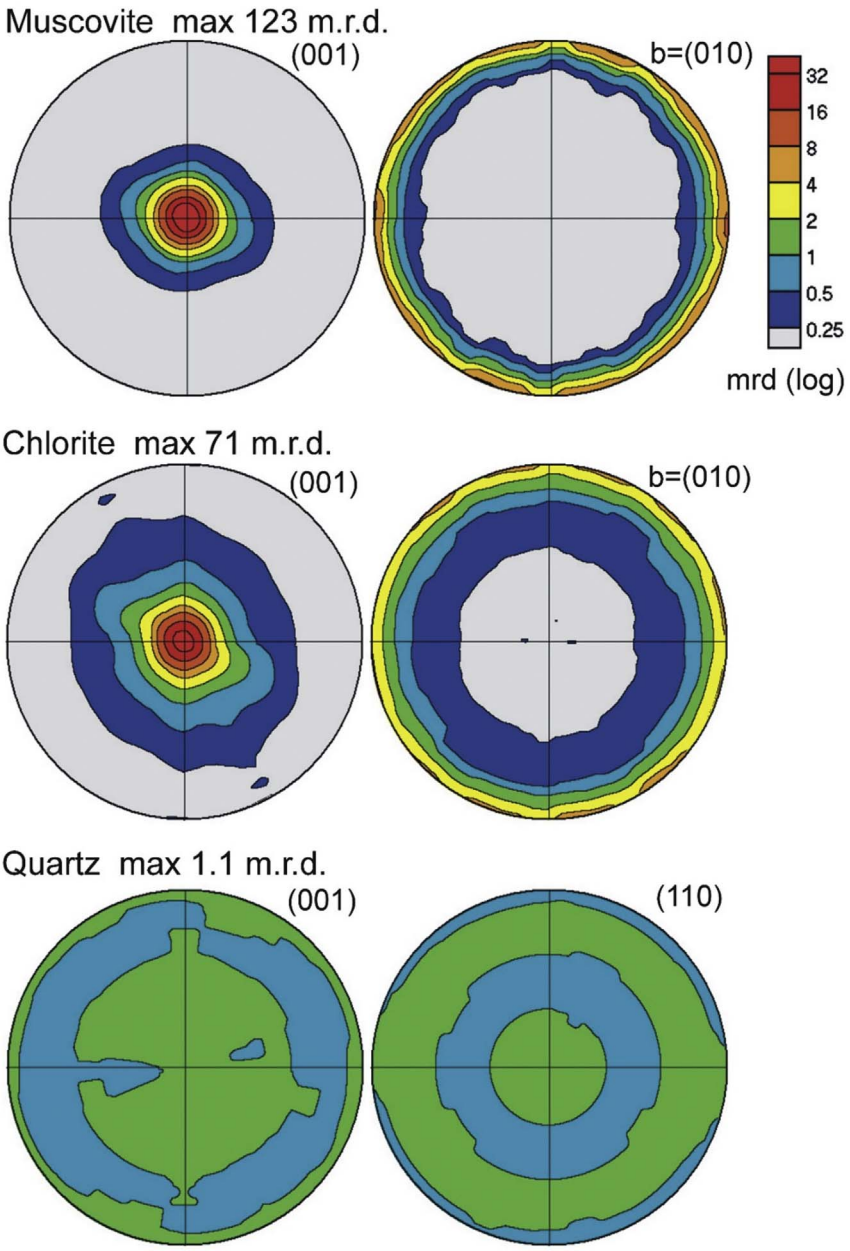

Fig. 5. Pole figures of muscovite, chlorite, and quartz projected on the foliation plane. Equal area projection, log scale for pole densities in multiples of random distribution (m.r.d.).

Table 1
Summary of tomography and Rietveld analysis: Composition (volume %), CPO (ODF maximum, (001) maximum-minimum, in m.r.d.), and 3D aspect ratio of La Fortelle slate.

	Volume %		ODF	(001)		3D aspect
	Tomography	Rietveld	maximum	maximum	minimum	ratio
Muscovite	36	28	195	123	0.01	2.7
Chlorite	17	23	141	71	0.11	2.9
Quartz	47	49	1.2	1.1	0.9	2.7

was performed at beamline 8.3.2 of the Advanced Light Source, operated for the DOE Office of Science by Lawrence Berkeley National Laboratory under Contract No. DE-AC02-05CH11231. SEM measurements were done at EPS-Berkeley. We are grateful to Tim Teague who helped with sample preparations. The sample was collected during a fieldtrip with Manuel Sintubin, Leuven. We are appreciative for discussions with Bevis Hutchinson and constructive comments from the editor Toru Takeshita and two reviewers that helped us improve the manuscript.

References

Aleksandrov, K.S., Ryzhova, T.V., 1961. The elastic properties of rock-forming minerals, II: layered silicates. Bull. Acad. Sci. USSR 12, 1799–1804.

Antao, S.M., Hassan, I., Wang, J., Lee, P.L., Toby, B.H., 2008. State-of-the-art high-resolution powder X-ray diffraction (HRPXRD) illustrated with Rietveld structure refinement of quartz, sodalite, tremolite, and meionite. Can. Mineral. 46, 1501–1509.

Bunge, H.-J., 1969. Mathematische Methoden der Texturanalyse. Akademie-Verlag, Berlin 330pp.

Cardenes, V., Rubio-Ordonez, A., Wichert, J., Cnuddle, J.P., Cnuddle, V., 2014. Petrography of roofing slates. Earth Sci. Rev. 138, 435–453.

Omalius d'Halloy, J. J. d', 1833. Introduction à la Géologie. Levrault, Paris.
Durney, D.W., 1976. Pressure solution and crystallization deformation. Phil. Trans. Roy. Soc. Lond. 208, 229–240.
Eberl, D.D., Velde, B., 1989. Beyond the Kübler index. Clay Miner. 24, 571–577.
Engelder, T., Geiser, P., Alvarez, W., 1980. Role of pressure solution and dissolution in geology. Geology 9, 44–45.
Guggenheim, S., Chang, Y.H., Koster van Groos, A.F., 1987. Muscovite dehydroxylation: high-temperature studies. Am. Mineral. 72, 537–550.
Haerinck, T., Wenk, H.-R., Debacker, T.N., Sintubin, M., 2015. Preferred mineral orientation of a chloritoid-bearing slate in relation to its magnetic fabric. J. Struct. Geol. 71, 125–135.
Ho, N.-C., van der Pluijm, B.A., Peacor, D.R., 2001. Static recrystallization and preferred orientation of phyllosilicates: michigamme Formation, northern Michigan, USA. J. Struct. Geol. 23, 887–893.
Hutchinson, W.B., 2012. The cube texture revisited. Proc. ICOTOM 16, Mumbai 2011. Mater. Sci. Forum 702–703, 3–10.
Hutchinson, W.B., Nes, E., 1992. Texture development during grain growth – a useful rule-of-thumb. Proc. Grain Growth in Polycrystalline Materials. Mater. Sci. Forum 94–96, 385–390.
Ishii, K., 1988. Grain growth and re-orientation of phyllosilicate minerals during the development of slaty cleavage in the South Kitakami Mountains, northeast Japan. J. Struct. Geol. 10, 145–154.
Jeffery, G.B., 1923. The motion of ellipsoidal particles immersed in a viscous fluid. Proc. Roy. Soc. Lond. 102, 161–179.
Kamb, W.B., 1959. Theory of preferred crystal orientation developed by crystallization under stress. J. Geol. 67, 153–170.
Kanitpanyacharoen, W., Parkinson, D.Y., de Carlo, F., Marone, F., Wenk, H.-R., MacDowell, A., Mokso, R., Stampanoni, M., 2013. A comparative study of X-ray microtomography on shales at different synchrotron facilities: ALS, APS and SLS. J. Synchrotron Radiat. 20, 1–9.
Knipe, R.J., 1981. The interaction of deformation and metamorphism in slates. Tectonophysics 78, 249–272.
Lutterotti, L., Vasin, R., Wenk, H.-R., 2014. Rietveld texture analysis from synchrotron diffraction images. I. Calibration and basic analysis. Powder Diffr. 29, 76–84.
March, A., 1932. Mathematische Theorie der Regelung nach der Korngestalt bei affiner Deformation. Z. Kristallogr. 81, 285–297.
Matthies, S., Vinel, G.W., 1982. On the reproduction of the orientation distribution function of textured samples from reduced pole figures using the concept of conditional ghost correction. Phys. Status Solidi B 112, K111–K114.
Merriman, R.J., Roberts, B., Peacor, D.R., 1990. A transmission electron microscope study of white mica crystallite size distribution in a mudstone to slate transitional sequence. Contrib. Mineral. Petrol. 106, 27–40.
Oertel, G., 1983. The relationship of strain and preferred orientation of phyllosilicate grains in rocks - a review. Tectonophysics 100, 413–447.
Oertel, G., Phakey, P.P., 1972. The texture of a slate from Nantlle, Caernarvon, North Wales. Texture 1, 1–8.
Ohno, I., Harada, K., Yoshitomi, C., 2006. Temperature variation of elastic constants of quartz across the $\alpha-\beta$ transition. Phys. Chem. Miner. 33, 1–9.
Ortoleva, P., Merino, E., Strickholm, P., 1982. Kinetics of metamorphic layering in anisotropically stressed rocks. Am. J. Sci. 282, 617–643.
Passchier, C.W., Trouw, R.A.J., 2005. Microtectonics, Second Ed. Springer Verlag, pp. 366pp.
Paterson, M.S., 1973. Nonhydrostatic thermodynamics and its geologic applications. Rev. Geophys. Space Phys. 11–2, 255–389.
Plessmann, W., 1966. Lösung, Verformung, Transport und Gefüge. Z. Dtsch. Geol. Ges. 115, 650–663.
Powell, C.McA., 1972. Tectonic dewatering and strain in the Michigamme slate. Michigan. Geol. Soc. Am. Bullet. 83, 2149–2158.
Rietveld, H.M., 1969. A profile refinement method for nuclear and magnetic structures. J. Appl. Crystallogr. 2, 65–71.
Rutter, E.H., 1976. The kinetics of rock deformation by pressure solution. Philoso. Trans. Royal Soc. A 283, 203–219.
Sander, B., 1950. Einführung in die Gefügekunde der geologischen Koerper, vol. 2 Springer Verlag, Vienna 409pp.
Schavemaker, Y.A., de Bresser, J.H.P., Van Baelen, H., Sintubin, M., 2012. Geometry and kinematics of the low-grade metamorphic 'Herbeumont shear zone' in the High-Ardenne slate belt (Belgium). Geol. Belg. 15, 126–136.
Shimizu, I., 1992. Nonhydrostatic and nonequilibrium thermodynamics of deformable materials. J. Geophys. Res. 97 (B4), 4587–4597.
Siddans, A.W.B., 1979. Deformation, metamorphism and texture development in Permian mudstones of the Glarus Alps (Eastern Switzerland). Eclogae Geol. Helv. 72, 601–621.
Tullis, T.E., 1976. Experiments on the origin of slaty cleavage and schistosity. Geol. Soc. Am. Bull. 87, 745–753.
van der Pluijm, B.A., Ho, N.-C., Peacor, D.R., Merriman, R.J., 1998. Contradictions of slate formation resolved? Nature 392 348–348.
Van Noten, K., Hilgers, C., Urai, J., Sintubin, M., 2012. The complexity of 3D stress-state changes during compressional tectonic inversion at the onset of orogeny. In: In: Healy (Ed.), Faulting, Fracturing, and Igneous Intrusion in the Erath's Crust, vol. 367. Geological Society London Special Publications, pp. 51–69.
Vaughan, M.T., Guggenheim, S., 1986. Elasticity of muscovite and its relationship to crystal structure. J. Geophys. Res. 91, 4657–4664.
Voisin, L., 1987. Les Ardoisieres de l'Ardenne. Editions Terres Ardennaises, Charleville-Mezieres.
Wagner, W., Le Bail, R., Hacar, M., Stanek, S., 1995. European roofing slates part 2: Geology of selected examples of slates deposits. Z. Angew. Geol. 41, 21–26.
Warr, L.N., Cox, S.C., 2016. Correlating illite (Kübler) and chlorite (Arkai) "crystallinity" indices with metamorphic mineral zones of South Island, New Zealand. Appl. Clay Sci. 134, 164–174.
Wenk, H.-R., Matthies, S., Donovan, J., Chateigner, D., 1998. BEARTEX: a Windows-based program system for quantitative texture analysis. J. Appl. Crystallogr. 31, 262–269.
Wenk, H.-R., Kanitpanyacharoen, W., Voltolini, M., 2010. Preferred orientation of phyllosilicates: comparison of fault gouge, shale and schist. J. Struct. Geol. 32, 478–489.
Wenk, H.-R., Lutterotti, L., Kaercher, P., Kanitpanyacharoen, W., Miyagi, L., Vasin, R., 2014. Rietveld texture analysis from synchrotron diffraction images. II. Complex multiphase materials and diamond anvil cell experiments. Powder Diffr. 29, 220–232.
Wood, D.S., Oertel, G., 1980. Deformation in the Cambrian slate belt of Wales. J. Geol. 88, 309–326.
Zanazzi, P.F., Montagnoli, M., Nazzareni, S., Comodi, S., 2007. Structural effects of pressure on monoclinic chlorite: a single crystal study. Am. Mineral. 92, 655–661.